Original Article

Compressive sensing of wireless sensors based on group sparse optimization for structural health monitoring

Yuequan Bao[1,2], Zuoqiang Shi[3], Xiaoyu Wang[1,2] and Hui Li[1,2]

Abstract

Vibration signals of most civil infrastructures have sparse characteristics (i.e. only a few modes contribute to the vibration of the structures). Therefore, the vibration data usually have sparse representation. Additionally, the vibration data measured by the sensors placed on different locations of structure have almost the same sparse structure in the frequency domain. On basis of the group sparsity of the structural vibration data, we proposed a group sparse optimization algorithm based on compressive sensing for wireless sensors. Different from the Nyquist sampling theorem, the data are first acquired by a nonuniform low-rate random sampling method according to compressive sensing theory. We then developed the group sparse optimization algorithm to reconstruct the original data from incomplete measurements. By conducting a field test on Xiamen Haicang Bridge with wireless sensors, we illustrate the effectiveness of the proposed approach. The results show that smaller reconstruction errors can be achieved using data from multiple sensors with the group sparse optimization method than using data from only single sensor. Even using only 10% random sampling data, the original data can be reconstructed using the group sparse optimization method with a small reconstruction error. In addition, the modal parameters can also be identified from the reconstruction data with small identification errors.

Keywords

Structural health monitoring, compressive sensing, data reconstruction, group sparse optimization, wireless sensor

Introduction

Wireless sensors and sensor networks for structural health monitoring

Structural health monitoring (SHM) technology was developed several decades ago, and a lot of civil infrastructures have been installed with some SHM systems all over world.[1–4] In a wired sensors–based SHM system, the wired connection between sensors and the data acquisition system increases the system cost and causes great difficulties for maintenance and replacement. As reported, the wired monitoring system on the Bill Emerson Memorial Bridge in Cape Girardeau, MO, USA, costs more than US$15,000 per sensor,[5] and a large portion of that cost was related to the wired data transmission cables. Wireless sensors and the wireless network have intelligent data processing capabilities with an embedded algorithm that do not have cables, which greatly reduces the sensor's installation cost. In comparison with traditional wired sensor–monitoring

systems, wireless sensors and wireless networks possess several advantages that make them attractive alternatives for monitoring large civil infrastructure.

In SHM, great efforts have been made to explore wireless sensing systems. Some academic and commercial smart sensor prototypes have been developed and used in the field of SHM.[6–13] Straser and Kiremidjian[6] first developed smart wireless sensors for application in civil engineering structures. A more exhaustive review is

[1]Key Lab of Structures Dynamic Behavior and Control of the Ministry of Education, Harbin Institute of Technology, Harbin, China
[2]School of Civil Engineering, Harbin Institute of Technology, Harbin, China
[3]Yau Mathematical Sciences Center, Tsinghua University, Beijing, China

Corresponding author:
Hui Li, Key Lab of Structures Dynamic Behavior and Control of the Ministry of Education, Harbin Institute of Technology, Harbin 150090, China.
Email: lihui@hit.edu.cn

given by Lynch and Loh[7] and Spencer et al.[8] Recently, wireless sensors have been used on many bridges for SHM purposes. On Jindo Bridge, a cable-stayed bridge in Korea, 70 Imote2 smart wireless sensors have been installed for SHM.[9] On Geumdang Bridge, a continuous beam bridge, Lynch et al.[10] installed 28 wireless sensors for SHM. The Stork Bridge in Switzerland,[11] Ferriby Road Bridge in England,[12] and Rock Island Arsenal Government Bridge in the United States[13] are all installed with some wireless sensor–based SHM system.

Compared with wired sensors, wireless sensor and sensor networks need additional energy acquisition technology to ensure the power supply to the sensors. In addition, in the long-term monitoring of the structure, large amounts of data acquisition and wireless transmission likely cause the instability of the wireless sensor networks. The wireless data transmission process will consume most of the energy of the sensor battery. Therefore, it is necessary to embed a data compression algorithm to reduce the amount of data transmission as much as possible to minimize energy consumption and prolong the service life of wireless sensor. The traditional data compression method, which is based on the sampling theorem, has its limitations: it first completes data collection, and then it compresses the data. For wireless sensors, the data compression process consumes part of the energy. Therefore, new data compression methods are needed to effectively improve the wireless sensors and wireless sensor network for long-term SHM.

Compressive sensing for wireless sensors and SHM

To avoid information loss when uniformly sampling a signal, the Shannon–Nyquist sampling theorem requires a sampling frequency at least two times that of the signal's bandwidth. For high-frequency signals, long-term real-time SHM with uniform sampling produces a large volume of data and results in the high cost of data sampling, storage, and transmission.

Compressive sensing (CS) provides a new sampling theory to reduce data acquisition when using the nonuniform low-rate random sampling method, which said that the sparse or compressible signals can be exactly reconstructed from highly underdetermined sets of measurements under the assumption of signal sparsity and under certain conditions on the measurement matrix.[14,15] The potential of CS for SHM has been investigated widely, and many CS applications have been presented. Bao et al.[16] investigated the CS for the acceleration data collection of SHM, finding that the sparsity of the vibration acceleration response data of the structures is the main factor affecting data reconstruction accuracy. Mascarenas et al.[17] studied the

compressed sensing techniques to detect structure damage. In their research, they developed compressed sensor to collect compressed coefficients from measurements and send them to an off-board processor for signal reconstruction using l_1 norm minimization; then, they implemented a compressed version of the matched filter onboard the sensor node to detect structural damage. Peckens and Lynch[18] proposed a bio-inspired CS technique to acquire data for SHM. O'Connor et al.[19] explored CS to reduce power consumption in wireless sensors for SHM. They modified the wireless sensor node to perform random sampling of data according to CS theory. Then, the randomly sampled data were transmitted off-site to a computational server for data reconstruction using the compressive sampling matching pursuit (CoSaMP) recovery algorithm and were processed further to extract the structure's mode shapes. Bao et al.[20] explored the use of CS to recover the lost data collected by wireless sensors for SHM, in which the random lost data are equivalent to the compressed CS data. The lost data were reconstructed using the sparse optimization method with high accuracy. Furthermore, they embedded the CS-based algorithm into Imote2 wireless sensor using a random demodulator technique; the field test results on the Songpu Bridge in Harbin, China, showed the successful recovery of the lost CS-based data.[21]

The CS method has been explored not only for data acquisition but also for structural modal identification, structural damage identification, and loads identification. Park et al.[22] proposed a novel method for modal identification directly using compressed sensing measurements. Yang and Nagarajaiah[23] proposed an output-only modal identification method combined with blind source separation (BSS) techniques and CS. In this method, the nonuniform low-rate random samples are used directly for modal identification. Wang and Hao[24] proposed a new CS-based damage identification scheme by damage identification problems as pattern classification problems. On the basis of the sparsity symposium of structural damage, the l_1 sparse optimization methods of CS theory also are used to identify structural damage.[25–27] In addition, Bao et al.[28] presented a sparse optimization of CS theory–based approach to identify the distribution of moving heavy vehicle loads on cable-stayed bridges.

In SHM, not only do most vibration signals of civil infrastructures have sparse characteristic but also the measured vibration data at different locations of the structure have a similar sparse structure in the frequency domain. In this article, we call this property group sparsity. To further increase the data reconstruction accuracy of CS in SHM, the group sparsity of data from multiple sensors is explored to form a group sparse optimization method for high-accuracy

reconstruction of compressed sampling data by wireless sensors. This group sparsity has been exploited in different areas and also has different names in different applications, including, for instance, joint sparsity,[29,30] simultaneous sparsity,[31,32] and group least absolute shrinkage and selection operator (LASSO).[33] In SHM, Yang and Nagarajaiah[34] proposed a data recovery method of structural vibration responses resulting from incomplete data. This method used the data from multiple sensors to form a low-rank matrix to recover the missing data. In their approach, however, the group sparsity of multiple sensors vibration data is not mentioned. In this article, using the special structure of the Fourier basis, we develop an efficient algorithm based on the augmented Lagrange multiplier (ALM) method. In this algorithm, only fast Fourier transform (FFT) or soft shrinkage is involved, making this method efficient. Section "CS based on group sparse optimization algorithm" gives the details of this algorithm.

CS based on group sparse optimization algorithm

Principle of the method

Unlike traditional Nyquist uniform sampling, the CS enables nonuniform low-rate random sampling as shown in Figure 1. The Nyquist sampling needs to sense N samples of a signal to avoid information loss as shown in Figure 1(a); however, CS randomly senses much fewer $M \ll N$, as shown in Figure 1(b). According to the CS theory, if the original signal is sparse, CS is able to exactly recover it from far fewer incoherent random measurements than what is required by the Shannon sampling theorem.

Suppose that K sensors are implemented in the structure. The acceleration is measured at discrete time t_j, $j = 1, \ldots, M$ by each sensor. Here, we assume the entire time span of the samples is $[0, T]$, and the sample time is distributed uniformly, that is, $t_j = jT/M$, $j = 1, \ldots, M$. By

collecting all the data together, we get the $M \times K$ matrix, $\mathbf{U}$ as follows

$$\mathbf{U} = \begin{bmatrix} u_{11} & u_{12} & \cdots & u_{1K} \\ u_{21} & u_{22} & \cdots & u_{2K} \\ \vdots & \vdots & \ddots & \vdots \\ u_{N1} & u_{N2} & \cdots & u_{NK} \end{bmatrix} \quad (1)$$

where u_{mk} is the data measured by the kth sensor at time t_m.

Then, the compressed sensing signal matrix, $\mathbf{U}$ is usually an incomplete matrix. Let $\Omega = \{(m, k) : U_{m,k}$ is available$\}$ and $P_\Omega : R^{M \times K} \to R^{M \times K}$ is the zero padding operator, that is, $\mathbf{Y} = P_\Omega \mathbf{U}$, as follows

$$y_{m,k} = \begin{cases} u_{m,k}, & (m, k) \in \Omega \\ 0, & \text{otherwise} \end{cases} \quad (2)$$

Then, the problem we are facing is how to calculate the original signal matrix $\mathbf{U}$ from the given signal $\mathbf{Y} = P_\Omega \mathbf{U} \in R^{M \times K}$

The signal matrix $\mathbf{U}$ can be represented as

$$\mathbf{U} = \mathbf{\Psi} \mathbf{X} \quad (3)$$

where $\mathbf{\Psi}$ is a Fourier matrix

$$\mathbf{\Psi} = \begin{bmatrix} e^{i2\pi t_1/T} & e^{i4\pi t_1/T} & \ldots & e^{i2M\pi t_1/T} \\ e^{i2\pi t_2/T} & e^{i4\pi t_2/T} & \ldots & e^{i2M\pi t_2/T} \\ \vdots & \vdots & \ddots & \vdots \\ e^{i2\pi t_M/T} & e^{i4\pi t_M/T} & \ldots & e^{i2M\pi t_M/T} \end{bmatrix} \quad (4)$$

where $\mathbf{X} \in C^{M \times K}$ are the Fourier coefficients of the original signal that has only a few nonzero rows. This representation gives us an alternative way to recover the signal matrix $\mathbf{U}$, which is so-called group sparsity. Generally speaking, a matrix $\mathbf{X}$ is said to be group sparse, if the entries of $\mathbf{X}$ are classified as many groups and only a few groups are nonzero. In different applications, the classification may be different. More
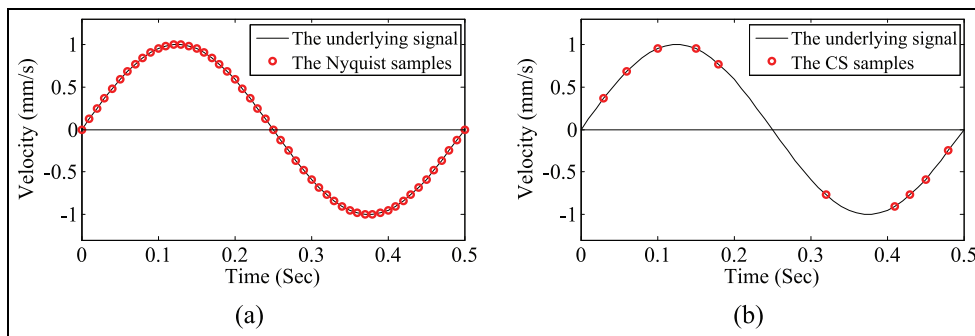

Figure 1. Nyquist sampling and CS sampling: (a) Nyquist samples and (b) CS samples.

precisely, in our application, one group corresponds to one row of $\mathbf{X}$.

Considering the measurement noise, equation (3) is changed to

$$\mathbf{U} = \mathbf{\Psi X} + \mathbf{\varepsilon} \qquad (5)$$

where $\mathbf{\varepsilon} \in R^{M \times K}$ is a Gaussian noise matrix.

The group sparse reconstruction problem has been well-studied recently in the literature.[29–33] A favorable approach is using the mixed $|| \cdot ||_{p,q}$ norm as regularization, where

$$\|\mathbf{X}\|_{p,q} = \left(\sum_{m=1}^{M} \|\mathbf{x}_m\|_p^q \right)^{1/q} \qquad (6)$$

One of the most popular choices of p, q is $p = 2$, $q = 1$, and we also use these values in this article. Then, the Fourier coefficients matrix $\mathbf{X}$ is recovered by solving the following optimization problem

$$\min_{\mathbf{X} \in C^{M \times K}} \|\mathbf{X}\|_{2,1} + \frac{\mu}{2} \|P_\Omega(\mathbf{\Psi X}) - P_\Omega \mathbf{U}\|_{Fro}^2 \qquad (7)$$

Once the optimal solution $\mathbf{X}_{rec}$ is obtained, the recovered signal matrix is given by

$$\mathbf{U}_{rec} = \mathbf{\Psi X}_{rec} \qquad (8)$$

Next, we will derive an efficient algorithm to solve the group sparse reconstruction problem in equation (7) based on the ALM[35] and split Bregman iteration.[36]

Algorithm

In this section, we give an iterative algorithm to solve the optimization problem of equation (7). First, we introduce an auxiliary variable $\mathbf{Z}$ to equation (7) as follows

$$\min_{\substack{\mathbf{X} \in R^{M \times K}, \\ \mathbf{Z} \in R^{M \times K}}} \|\mathbf{X}\|_{2,1} + \frac{\mu}{2} \|\mathbf{Z}\|_{Fro}^2, \text{subject to} : P_\Omega \mathbf{Z} = \mathbf{\Psi X} - P_\Omega \mathbf{U}$$
$$(9)$$

We next use the ALM algorithm to solve equation (9). The ALM algorithm solves a constrained problem by iteratively solving a sequence of unconstrained problem. For a general constrained optimization problem[35]

$$\min F(x), \text{subject to} : g(x) = 0 \qquad (10)$$

The ALM algorithm solves equation (10) by the following iterative process

$$x^k = \arg \min_x F(x) + \frac{\tau}{2} \left\| g(x) + \frac{\omega^k}{\tau} \right\|_2^2$$
$$\omega^{k+1} = \omega^k + \tau g(x^k)$$

where τ is a parameter in ALM. It is well-known that the convergence of ALM algorithm is robust to the choice of this parameter.

Applying the ALM algorithm to equation (9), we get an iterative algorithm

$$\left(\mathbf{X}^{k+1}, \mathbf{Z}^{k+1} \right) = \arg \min_{\substack{\mathbf{X} \in C^{M \times K}, \\ \mathbf{Z} \in R^{M \times K}}} \|\mathbf{X}\|_{2,1} + \frac{\mu}{2} \|P_\Omega \mathbf{Z}\|_{Fro} + \frac{\tau}{2}$$
$$\left\| \mathbf{Z} - \mathbf{\Psi X} + P_\Omega \mathbf{U} + \frac{\mathbf{Q}^k}{\tau} \right\|_{Fro}^2 \qquad (11)$$

$$\mathbf{Q}^{k+1} = \mathbf{Q}^k + \tau \left(\mathbf{Z}^{k+1} - \mathbf{\Psi X}^{k+1} + P_\Omega \mathbf{U} \right) \qquad (12)$$

To further simplify the algorithm, we use the split Bregman iteration[36] to compute $\mathbf{X}^{k+1}$, $\mathbf{Z}^{k+1}$ separately, as follows

$$\mathbf{X}^{k+1} = \arg \min_{\mathbf{W} \in C^{M \times K}} \|\mathbf{X}\|_{2,1} + \frac{\tau}{2} \left\| \mathbf{Z}^k - \mathbf{\Psi X} + P_\Omega \mathbf{U} + \frac{\mathbf{Q}^k}{\tau} \right\|_{Fro}^2$$
$$(13)$$

$$\mathbf{Z}^{k+1} = \arg \min_{\mathbf{Z} \in R^{M \times K}} \frac{\mu}{2} \|P_\Omega \mathbf{Z}\|_{Fro}^2 + \frac{\tau}{2}$$
$$\left\| \mathbf{Z} - \mathbf{\Psi X}^{k+1} + P_\Omega \mathbf{U} + \frac{\mathbf{Q}^k}{\tau} \right\|_{Fro}^2 \qquad (14)$$

$$\mathbf{Q}^{k+1} = \mathbf{Q}^k + \tau \left(\mathbf{Z}^{k+1} - \mathbf{\Psi X}^{k+1} + P_\Omega \mathbf{U} \right) \qquad (15)$$

Notice that both equations (13) and (14) have an explicit solver. In equation (13), using Parseval's equality in Fourier transform, we have

$$\mathbf{X}^{k+1} = \arg \min_{\mathbf{W} \in C^{M \times K}} \|\mathbf{X}\|_{2,1} + \frac{\tau}{2}$$
$$\left\| \mathbf{X}^k - \mathbf{\Psi}^{-1}(\mathbf{Z} + P_\Omega \mathbf{U}) + \frac{\mathbf{Q}^k}{\tau} \right\|_{Fro}^2 =$$
$$S_{1/\tau} \left(\mathbf{\Psi}^{-1} \left(\mathbf{Z}^k + P_\Omega \mathbf{U} + \frac{\mathbf{Q}^k}{\tau} \right) \right) \qquad (16)$$

where $S_{1/\tau} : R^{M \times K} \to R^{M \times K}$ is a shrink operator. Let $\mathbf{W}$ be the $M \times K$ matrix and $\mathbf{w}_j$, $j = 1, \ldots, M$ be rows of $\mathbf{W}$. For each $\mathbf{w} \in C^K$

$$S_\mu(\mathbf{w}) = \begin{cases} (\|\mathbf{w}\|_{Fro} - \mu) \frac{\mathbf{w}}{\|\mathbf{w}\|_{Fro}}, & \text{if} \|\mathbf{w}\|_{Fro} \geq \mu \\ 0, & \text{otherwise} \end{cases} \qquad (17)$$

Then, S_μ for matrix is defined as follows

$$S_\mu(\mathbf{W}) = \begin{bmatrix} S_\mu(\mathbf{w}_1) \\ S_\mu(\mathbf{w}_2) \\ \vdots \\ S_\mu(\mathbf{w}_M) \end{bmatrix} \qquad (18)$$

Direct calculation gives the formula of $\mathbf{Z}^{k+1}$ as follows

$$\mathbf{Z}^{k+1} = \mathbf{W}^{k+1} - \frac{\mu}{\mu+\tau} P_\Omega \mathbf{W}^{k+1} \qquad (19)$$

where

$$\mathbf{W}^{k+1} = \mathbf{\Psi}\mathbf{X}^{k+1} - P_\Omega \mathbf{U} - \frac{\mathbf{Q}^k}{t} \qquad (20)$$

Summarizing this derivation, we get an iterative algorithm to solve the optimization problem in equation (7). First, let $\mathbf{Q}^0 = \mathbf{Z}^0 = 0$ and choose a value of τ, and then conduct the following iteration until the solution converges

$$\mathbf{X}^{k+1} = S_{1/\tau}\left(\mathbf{\Psi}^{-1}\left(\mathbf{Z}^k + P_\Omega \mathbf{U} + \frac{\mathbf{Q}^k}{k}\right)\right) \qquad (21)$$

$$\mathbf{W}^{k+1} = \mathbf{\Psi}\mathbf{X}^{k+1} - P_\Omega \mathbf{U} - \frac{\mathbf{Q}^k}{k} \qquad (22)$$

$$\mathbf{Z}^{k+1} = \mathbf{W}^{k+1} - \frac{\mu}{\mu+\tau} P_\Omega \mathbf{W}^{k+1} \qquad (23)$$

$$\mathbf{Q}^{k+1} = \mathbf{Q}^k - \tau\left(\mathbf{\Psi}\mathbf{X}^{k+1} - \mathbf{Z}^{k+1} - P_\Omega \mathbf{U}\right) \qquad (24)$$

In this algorithm, only FFT, inverse FFT, and the simple shrink operator are used, which make this algorithm quite efficient.

Figure 2. Xiamen Haicang Bridge.

Field test of a bridge

Description of the test

We conducted a field test on Xiamen Haicang Bridge. The bridge is a steel-box-girder suspension bridge with a span distribution of 230 m + 648 m + 230 m, as shown in Figure 2. The bridge has two towers with a height of 140 m and the width of the bridge deck is 32 m. To avoid disturbing the normal traffic, the test is carried out at midnight. The test schemes are shown in Figure 3. The tests are repeated nine times and tested a total of 62 test points. Test 1 had seven test points (Nos 1–6 and No. 26); wireless sensors are placed on the seven test points to measure the vibration data. The time duration of each test was 20 min. After the test is completed, the wireless sensors were moved to Test 2, which also included seven test points (Nos 7–12 and No. 26). Considering the effective wireless data transmission distances, test point No. 26 was selected as the reference point for all tests. In the same way, Test 2 to Test 9 are conducted. The test used nine commercial wireless velocity sensors, as shown in Figure 4, and the sampling frequency for data acquisition was 100 Hz.
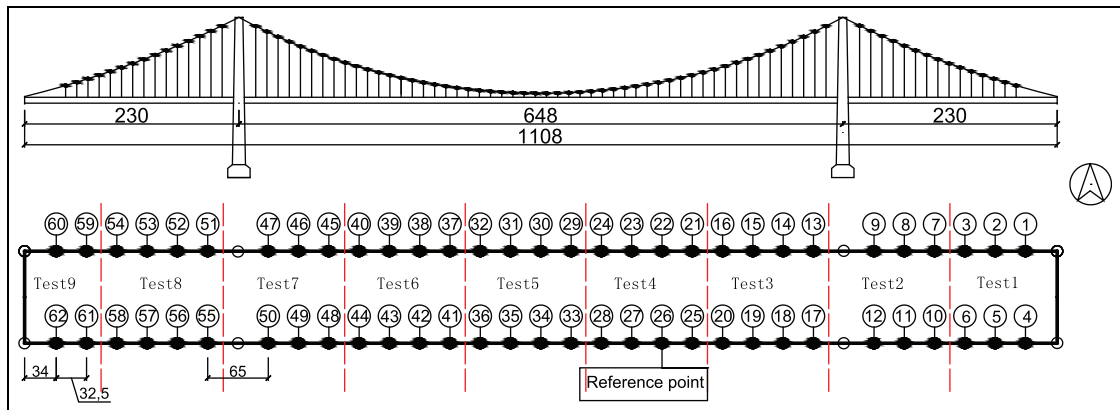

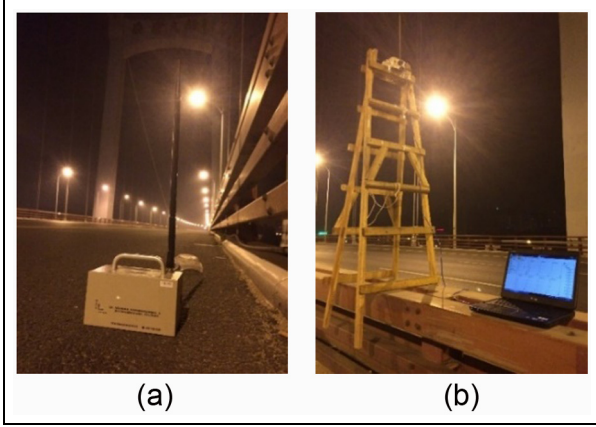**Figure 3.** The placement of test points.

Figure 4. (a) The wireless sensor node and (b) wireless base station.

The representative data sets measured from the bridge are shown in Figure 5(a). The Fourier spectrum at the measured response is shown in Figure 5(b), which shows that the data from multiple sensors almost have similar sparsity in the frequency domain. To further illustrate the similar sparsity of the data from multiple sensors, the cross-correlation of the Fourier amplitude spectrum is calculated by

$$\gamma_{XY} = \frac{\sum\limits_{i=1}^{N}(X_i - \bar{X})(Y_i - \bar{Y})}{\sqrt{\sum\limits_{i=1}^{N}(X_i - \bar{X})^2}\sqrt{\sum\limits_{i=1}^{N}(Y_i - \bar{Y})^2}} \tag{25}$$

Table 1 shows the results, which indicates that the minimal and maximal cross-correlation coefficients are 0.5117 and 0.9589, respectively. Most cross-correlation coefficients are within a range of [0.7, 0.95]. These cross-correlation coefficients further indicate the group sparsity of the signal.

Data sampling by CS

Because CS sensors are not yet commercially available, the behavior of CS sensors are simulated. The procedure of CS data sampling is shown in Figure 6, which demonstrates that data are randomly sampled.
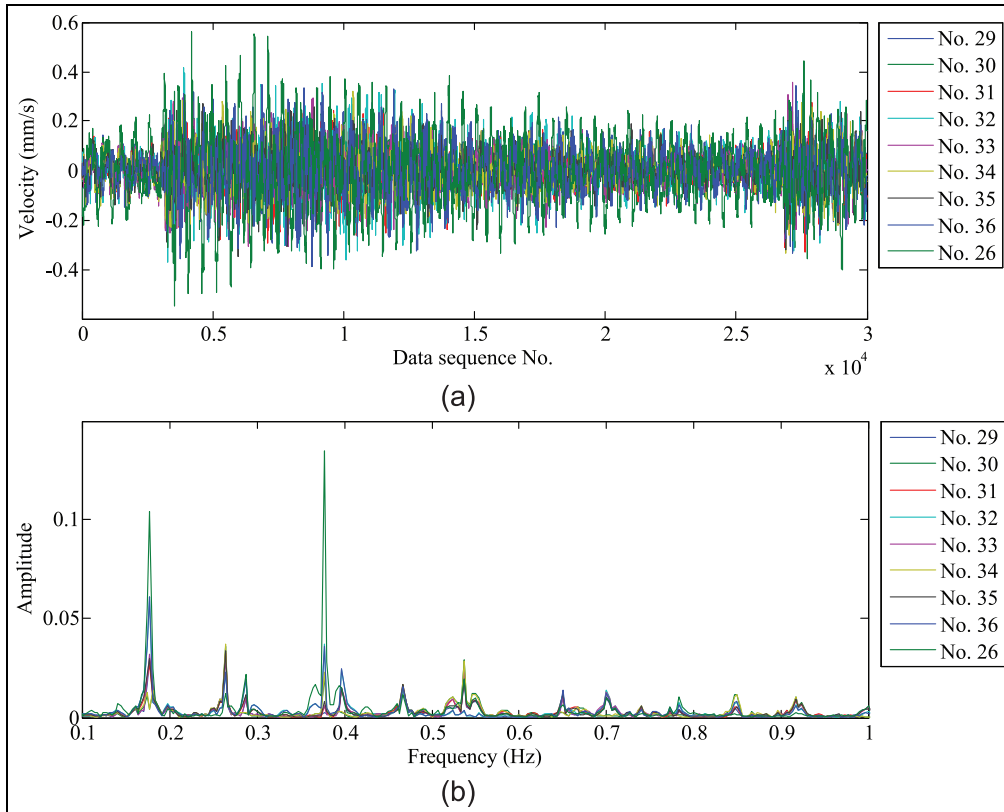

Figure 5. The typical measurements and Fourier spectrum: (a) the measured velocity data of test points Nos 29–36 and the reference point (No. 26) and (b) the Fourier spectrum of the measured velocity data of test points Nos 29–36 and the reference point (No. 26).

Table 1. The cross-correlation coefficients matrix of the Fourier amplitude spectrum of multiple sensors data.

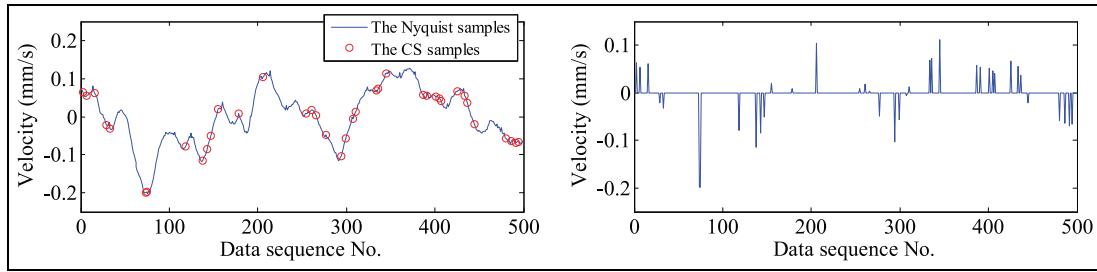|	No. 29	No. 30	No. 31	No. 32	No. 33	No. 34	No. 35	No. 36	No. 26
No. 29	I	0.7534	0.9392	0.8091	0.9544	0.7663	0.9588	0.7934	0.5693
No. 30		I	0.7542	0.6222	0.7618	0.9632	0.7704	0.6353	0.5117
No. 31			I	0.8227	0.9589	0.7720	0.9584	0.8139	0.5754
No. 32				I	0.8265	0.6459	0.8422	0.9477	0.7864
No. 33					I	0.7677	0.9481	0.8128	0.5875
No. 34						I	0.7770	0.6434	0.5344
No. 35							I	0.8324	0.6127
No. 36								I	0.8012
No. 26									I

Figure 6. The procedure of CS data sampling.

The typical measured velocity data by wireless sensor are shown in Figure 7(a). We simulate the nonuniform low-rate random sampling of CS, and the data with 10%, 20%, and 30% samples are shown in Figure 7(b) to (d).

Data reconstruction results

The data reconstruction results for 10%, 20%, and 30% samples are shown in Figures 8 to 10, respectively. Figures 8(a), 9(a) and 10(a) are the reconstruction results using data from one sensor, and Figures 8(b), 9(b) and 10(b) are the reconstruction results using data from multiple sensors (nine sensors). These figures show that the smaller reconstruction errors can be achieved by considering data from multiple sensors using the group sparse optimization method.

To investigate the relation between sampling ratio and reconstruction error, the sampling ratios 10%, 15%, 20%, 25%, and 30% are considered. The reconstruction error is calculated by

$$\xi = \frac{\|\hat{u} - u\|_2}{\|u\|_2} \qquad (26)$$

where $\hat{u}$ and u are the reconstruction data and the original data, respectively. The results of the data reconstruction error of the data taken from the nine sensors in Test 5 are shown in Figure 11, illustrating that
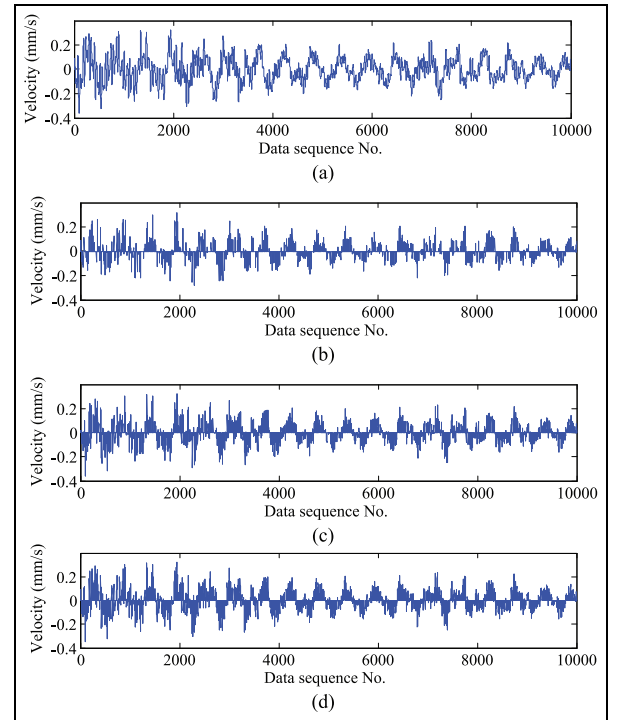

Figure 7. The sampling data by CS: (a) original data, (b) 10% samples, (c) 20% samples, and (d) 30% samples.

reconstruction errors decrease with an increase in the data sampling ratios for both the data from the single
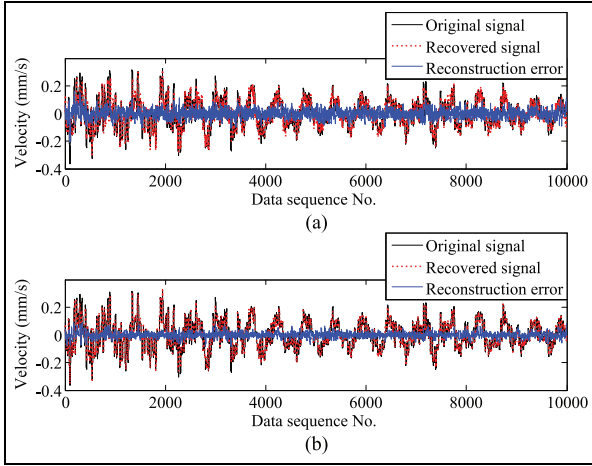
Figure 8. Data reconstruction results from 10% samples: (a) reconstruction from single sensor data and (b) reconstruction from multiple sensors data.
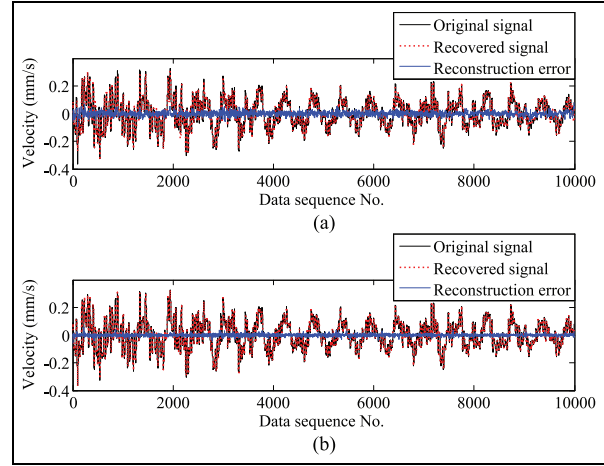

Figure 10. Data reconstruction results from 30% samples: (a) reconstruction from single sensor data and (b) reconstruction from multiple sensors data sets.
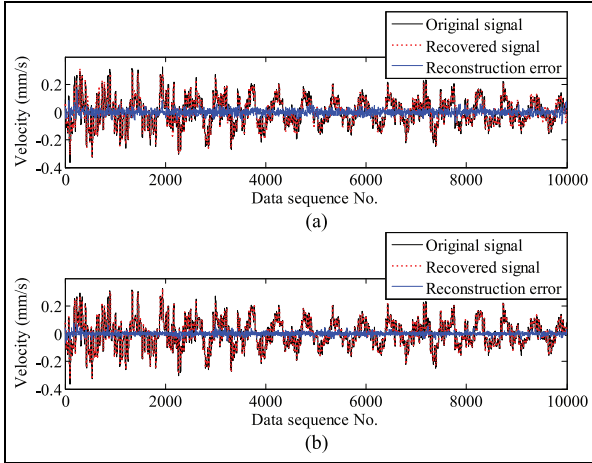

Figure 9. Data reconstruction results from 20% samples: (a) reconstruction from single sensor data and (b) reconstruction from multiple sensors data sets.

sensor and the data from the multiple sensors using group sparse optimization method. In addition, the reconstruction errors using multiple sensors data by group sparse optimization method are less than those of using single sensor. These errors further indicate that the group sparsity of the data from multiple sensors can effectively increase the accuracy of CS data reconstruction.

Figure 12 shows the relationships of the reconstruction error with the sensor number used in data reconstruction based on the group sparse optimization method under different sampling ratios. It is evident that the reconstruction error decreases as the number of sensors increases under different sampling ratios from 10% to 30%.

The reconstruction errors in the time and frequency domain of all test points data are shown in Figures 13 and 14, respectively. These figures show that multiple sensors data–based group sparse optimization method obviously decreases the data reconstruction error in both the time and frequency domain. In the case of 10% samples, the minimal reconstruction error in all reconstruction data using multiple sensors data–based group sparse optimization method is 0.0717, which is much lower than the 0.1401 following the method based on a single sensor. In the case of 30% samples, the minimal reconstruction error using multiple sensors data–based group optimization method is 0.0344; however, the error following the method based on a single sensor is 0.0826.

Modal identification results

The power spectral densities (PSD) of the original signal and the reconstruction signal with 10% random samples are shown in Figure 15. It is evident that PSD results from reconstruction signal using data from the single sensor and the reconstruction signal using data from multiple sensors are quite close to those of the original.

To investigate the influences of the data reconstruction error on the modal identification results, the modal frequencies and mode shapes identified by the natural excitation technique (NExT)[37] and combined with eigensystem realization algorithm (ERA) methods[38] are shown in Tables 2 and 3 and Figure 16, respectively. The theoretical frequencies and mode shapes are calculated from the finite element model of the bridge. The modal assurance criterion (MAC) values of the mode shapes are calculated by
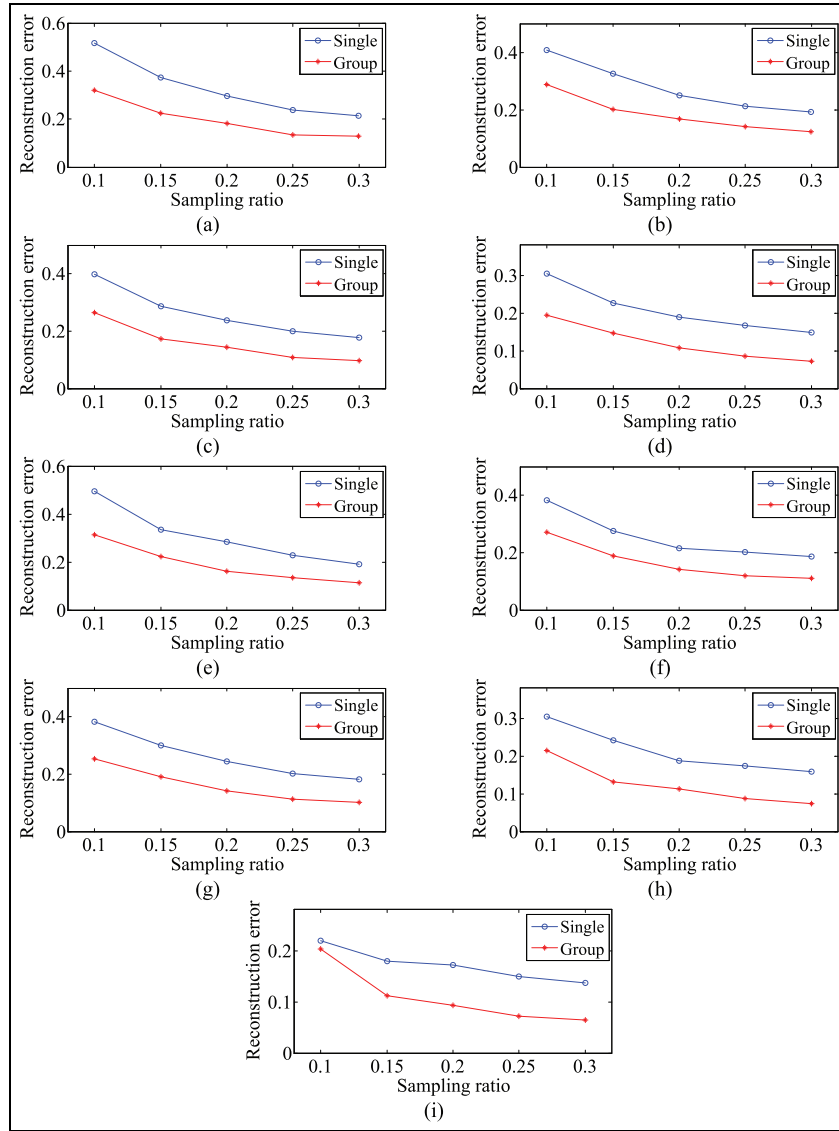
Figure 11. The reconstruction errors with different sampling ratios: (a) test point 33, (b) test point 34, (c) test point 35, (d) test point 36, (e) test point 37, (f) test point 38, (g) test point 39, (h) test point 40, and (i) test point 26 (reference point).
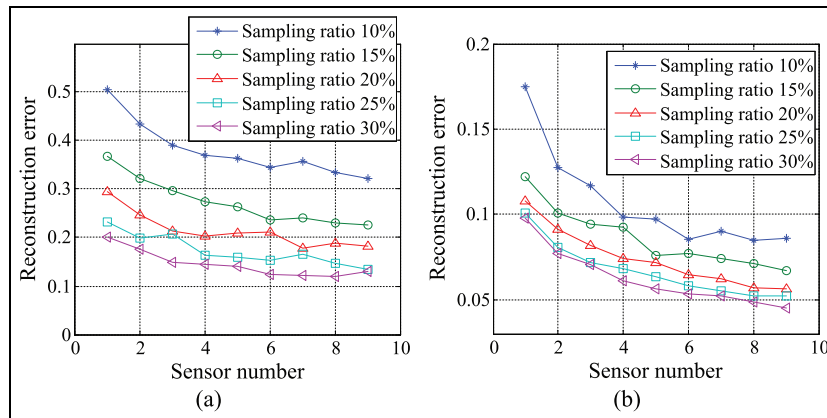

Figure 12. The relationship of the reconstruction error with sensor number: (a) Test 5 and (b) Test 6.
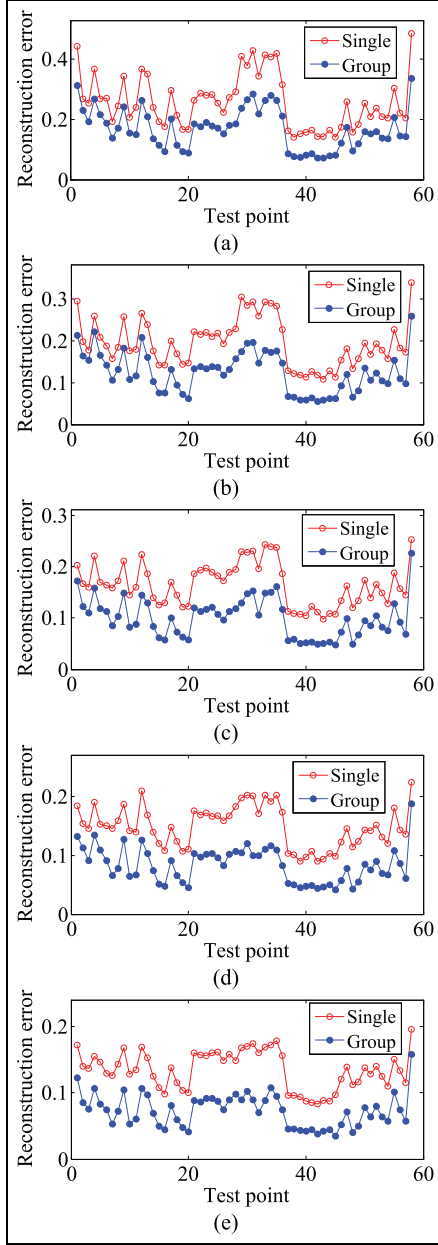
Figure 13. Reconstruction error in the time domain of all test points data: (a) 10% samples, (b) 15% samples, (c) 20% samples, (d) 25% samples, and (e) 30% samples.

Figure 14. Reconstruction error in the frequency domain of all test points data: (a) 10% samples, (b) 15% samples, (c) 20% samples, (d) 25% samples, and (e) 30% samples.

$$\mathrm{MAC} = \frac{\left(\varphi_r^T \hat{\varphi}_r\right)^2}{\left(\varphi_r^T \hat{\varphi}_r\right)\left(\varphi_r^T \hat{\varphi}_r\right)} \quad r = 1, 2, \cdots n \quad (27)$$

where φ_r and $\hat{\varphi}_r$ are the rth theoretical and identified mode shape, respectively.

The results show that the identified first two frequencies and mode shapes from the reconstruction data are almost consistent with the identification results from original data. This illustrates that the data reconstruction errors of both the single and multiple sensors
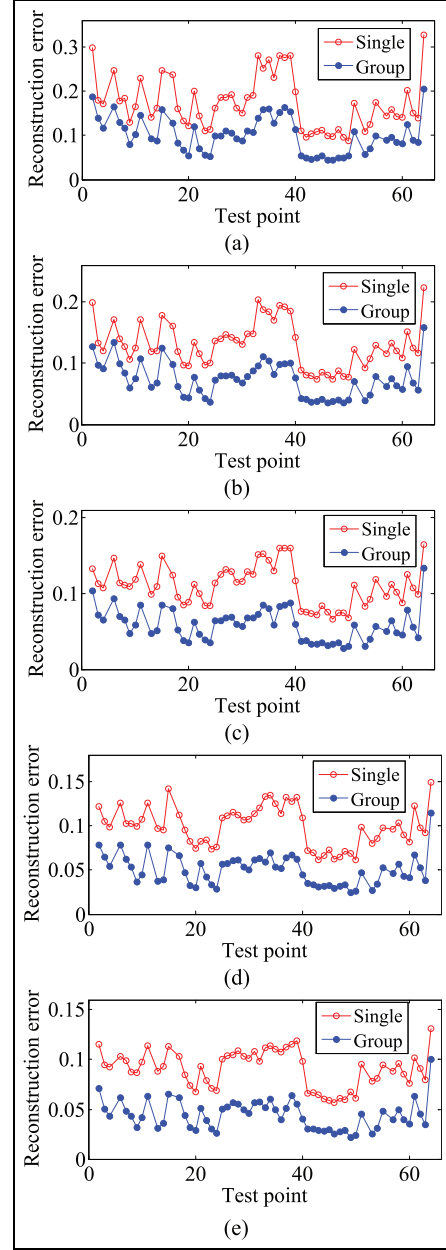
data–based methods have less impact on modal identification results.

Conclusion

In this article, we first proposed a group sparse optimization method for CS data reconstruction of wireless sensors for SHM. This method considers the group sparsity of structural vibration data from multiple sensors in the frequency domain to form a data
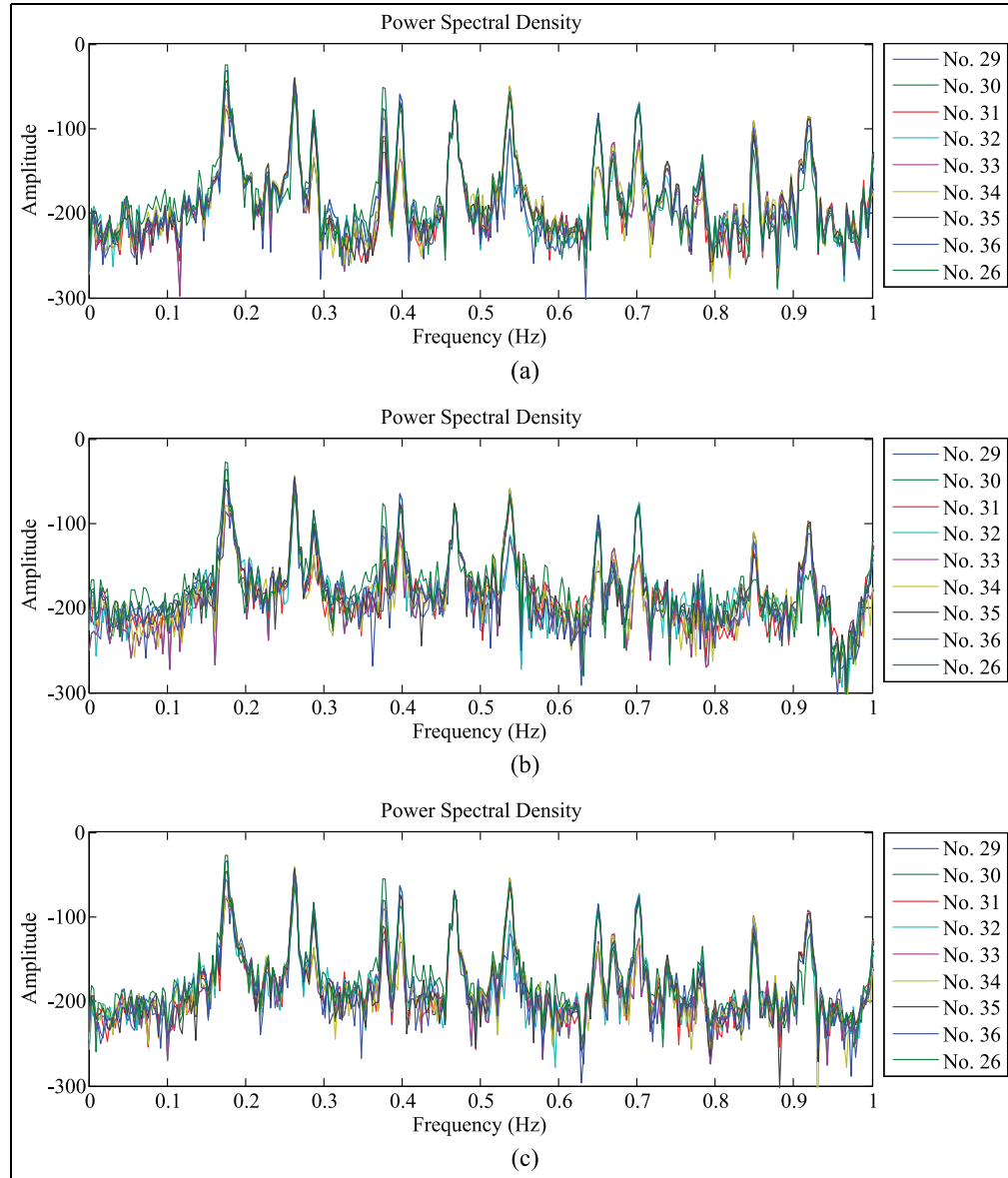
Figure 15. The PSDs of the original signal and reconstruction signal: (a) original signal, (b) reconstruction signal from single sensor data with 10% samples, and (c) reconstruction signal from group sensors data with 10% samples.

Table 2. Frequency.

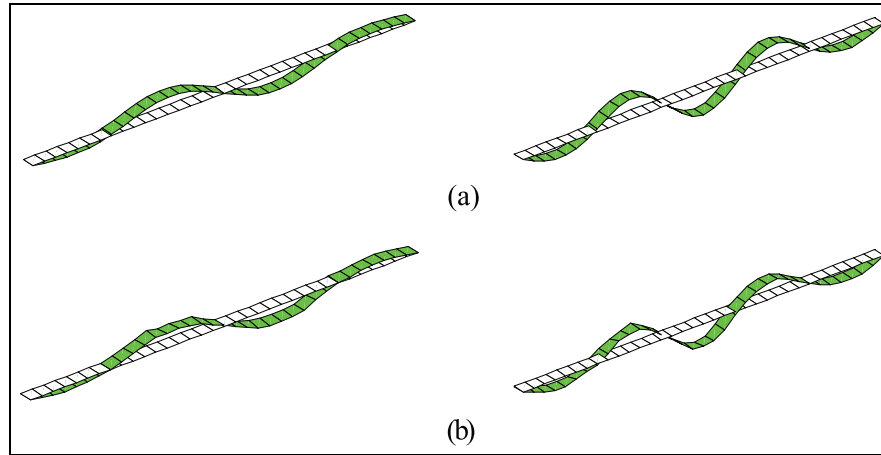| No.	Theoretical	Identified from original data	Identified from reconstruction data					
			10%		20%		30%	
			Single	Group	Single	Group	Single	Group
1	0.2199	0.2049	0.2033	0.2039	0.2040	0.2034	0.2049	0.2050
2	0.3196	0.2816	0.2835	0.2829	0.2821	0.2822	0.2815	0.2818

Figure 16. The first two identified mode shapes: (a) identification results by original signal and (b) identification results by reconstruction signal from group sensors data with 10% samples.

Table 3. MAC.

No.	Identified from original data	Identified from reconstruction data					
		10%		20%		30%	
		Single	Group	Single	Group	Single	Group
1	0.9877	0.8126	0.8688	0.9671	0.9845	0.9792	0.9808
2	0.9807	0.8428	0.9175	0.8192	0.8690	0.9607	0.9700

MAC: modal assurance criterion.

reconstruction optimization problem under a group LASSO framework. For the specific problem considered in this article, an efficient algorithm based on ALM and split Bregman iteration is developed. In this algorithm, we need to calculate only an FFT and simple shrink operation, making the computation quite fast. To verify the proposed method, we conducted field tests on Xiamen Haicang Bridge using wireless sensors. The following conclusions can be drawn:

1. The data from multiple sensors have similar sparsity in the frequency domain. This group sparsity is verified by the cross-correlation coefficients, which have values within the range of [0.7, 0.95]. This indicates that the data have strong correlation in the frequency domain.
2. The vibration data reconstruction results show that the highly incomplete random sampling data can be well-reconstructed using the group sparse optimization method. Even using 10% random sampling data, the original data can be reconstructed by the group sparse optimization method with a small reconstruction error. In both the time and frequency domain, the reconstruction errors of the multiple sensors data–based group sparse

optimization method are all less than the single sensor data–based optimization method.
3. The modal identification results show that the identified frequencies and mode shapes from the reconstruction data are almost consistent with the identification results from the original data, which indicates that the reconstruction errors of both the single and multiple sensors data–based methods have less impact on modal identification results.
4. The proposed method can be used for compressive sampling of structural vibration data. The effectiveness for other types of data, such as strain and displacement, still need to be investigated. Additionally, the group sparsity of the vibration data found in this study will be a useful feature in many SHM inverse problems. The proposed group sparse optimization method can also be used to recover the missing data from wireless sensors and sensor networks and for SHM error data correction. These applications will be studied in the future.

Declaration of conflicting interests

The author(s) declared no potential conflicts of interest with respect to the research, authorship, and/or publication of this article.

References

1. Ou J and Li H. Structural health monitoring in mainland China: review and future trends. *Struct Health Monit* 2010; 9(3): 219–232.
2. Li H and Ou J. The state of the art in structural health monitoring of cable-stayed bridges. *J Civil Struct Health Monit* 2016; 6(1): 43–67.
3. Li HN, Ren L, Jia ZG, et al. State-of-the-art in structural health monitoring of large and complex civil infrastructures. *J Civil Struct Health Monit* 2016; 6: 3–16.
4. Mufti AA. Structural health monitoring of innovative Canadian civil engineering structures. *Struct Health Monit* 2002; 1(1): 89–103.
5. Celebi M. Real-time seismic monitoring of the New Cape Girardeau Bridge and preliminary analyses of recorded data: an overview. *Earthq Spectra* 2006; 22(3): 609–630.
6. Straser EG and Kiremidjian AS. A modular visual approach to damage monitoring for civil structures. *Proc SPIE* 1996; 2719: 112–122.
7. Lynch JP and Loh KJ. A summary review of wireless sensors and sensor networks for structural health monitoring. *Shock Vib Digest* 2006; 38(2): 91–130.
8. Spencer BF Jr, Jo H, Mechitov KA, et al. Recent advances in wireless smart sensors for multi-scale monitoring and control of civil infrastructure. *J Civil Struct Health Monit* 2016; 6(1): 17–41.
9. Jang S, Jo H, Cho S, et al. Structural health monitoring of a cable-stayed bridge using smart sensor technology: deployment and evaluation. *Smart Struct Syst* 2010; 6(5–6): 439–459.
10. Lynch JP, Wang Y, Loh KJ, et al. Performance monitoring of the Geumdang Bridge using a dense network of high-resolution wireless sensors. *Smart Mater Struct* 2006; 15: 1561–1575.
11. Meyer J, Bischoff R, Feltrin G, et al. Wireless sensor networks for long-term structural health monitoring. *Smart Struct Syst* 2010; 6(3): 263–275.
12. Hoult NA, Fidler PRA, Hill PG, et al. Long-term wireless structural health monitoring of the Ferriby Road Bridge. *ASCE J Bridge Eng* 2010; 15(2): 153–159.
13. Cho S, Giles RK and Spencer BF. System identification of a historic swing truss bridge using a wireless sensor network employing orientation correction. *Struct Control Health Monit* 2015; 22(2): 255–272.
14. Donoho D. Compressed sensing. *IEEE T Inform Theory* 2006; 52(4): 1289–1306.
15. Candès EJ. Compressive sampling. In: *Proceedings of the international congress of mathematicians*, Madrid, 22–30 August 2006.
16. Bao Y, Beck JL and Li H. Compressive sampling for accelerometer signals in structural health monitoring. *Struct Health Monit* 2011; 10(3): 235–246.
17. Mascarenas D, Cattaneo A, Theiler J, et al. Compressed sensing techniques for detecting damage in structures. *Struct Health Monit* 2013; 12(4): 325–338.
18. Peckens CA and Lynch JP. Utilizing the cochlea as a bio-inspired compressive sensing technique. *Smart Mater Struct* 2013; 22(10): 105027.
19. O'Connor SM, Lynch JP and Gilbert AC. Compressed sensing embedded in an operational wireless sensor network to achieve energy efficiency in long-term monitoring applications. *Smart Mater Struct* 2014; 23: 085014.
20. Bao Y, Li H, Sun X, et al. Compressive sampling based data loss recovery for wireless sensor networks used in civil structural health monitoring. *Struct Health Monit* 2013; 12(1): 78–95.
21. Zou Z, Bao Y and Li H. Embedding compressive sensing based data loss recovery algorithm into wireless smart sensors for structural health monitoring. *IEEE Sens J* 2014; 15(2): 797–808.
22. Park JY, Wakin MB and Gilbert AC. Modal analysis with compressive measurements. *IEEE T Signal Proces* 2014; 62(7): 1655–1670.
23. Yang Y and Nagarajaiah S. Output-only modal identification by compressed sensing: non-uniform low-rate random sampling. *Mech Syst Signal Pr* 2015; 56: 15–34.
24. Wang Y and Hao H. Damage identification scheme based on compressive sensing. *ASCE J Comput Civil Eng* 2013; 29(2): 04014037.
25. Zhou S, Bao Y and Li H. Structural damage identification based on substructure sensitivity and l1 sparse regularization. In: *Proceedings of SPIE smart structures and materials + nondestructive evaluation and health monitoring*, San Diego, CA, 10–14 March 2013.
26. Zhou XQ, Xia Y and Weng S. L1 regularization approach to structural damage detection using frequency data. *Struct Health Monit* 2015; (14): 6571–6582.
27. Zhang CD and Xu YL. Comparative studies on damage identification with Tikhonov regularization and sparse regularization. *Struct Control Health Monit* 2016; 23(3): 560–579.
28. Bao Y, Li H, Chen Z, et al. Sparse l1 optimization-based identification approach for the distribution of moving heavy vehicle loads on cable-stayed bridges. *Struct Control Health Monit* 2016; 23(1): 144–155.
29. Fornasier M and Rauhut H. Recovery algorithms for vector valued data with joint sparsity constraints. *SIAM J Numer Anal* 2008; 46(2): 577–613.
30. Mishali M and Eldar YC. Reduce and boost: recovering arbitrary sets of jointly sparse vectors. *IEEE T Signal Proces* 2008; 56(10): 4692–4702.
31. Tropp JA, Gilbert AC and Strauss MJ. Algorithms for simultaneous sparse approximation, part I: greedy pursuit. *Signal Process* 2006; 86: 572–588.
32. Tropp JA. Algorithms for simultaneous sparse approximation, part II: convex relaxation. *Signal Process* 2006; 86: 589–602.
33. Ming Y and Lin Y. Model selection and estimation in regression with grouped variables. *J R Stat Soc Ser B Stat Methodol* 2006; 68(1): 49–67.
34. Yang Y and Nagarajaiah S. Harnessing data structure for recovery of randomly missing structural vibration

responses time history: sparse representation versus low-rank structure. *Mech Syst Signal Pr* 2016; 74: 165–182.

35. Bertsekas D. *Constrained optimization and Lagrange multiplier method.* Cambridge, MA: Academic Press, 1982.

36. Goldstein T and Osher S. The split Bregman method for L1-regularized problems. *SIAM J Imaging Sci* 2009; 2: 323–343.

37. James GH, Carne TG and Lauffer JP. The natural excitation technique (NExT) for modal parameter extraction from operating structures. *Modal Anal Int J Anal Exp Modal Anal* 1995; 10(4): 260.

38. Juang JN and Pappa RS. An eigensystem realization algorithm for modal parameter identification and model reduction. *J Guid Control Dynam* 1985; 8(5): 620–627.